Comparing the Temperature-Dependent Conductance of the Two Structurally Similar *E. coli* Porins OmpC and OmpF

István Biró,[△] Soroosh Pezeshki,[△] Helge Weingart, Mathias Winterhalter,[*] and Ulrich Kleinekathöfer[*]
School of Engineering and Science, Jacobs University Bremen, Bremen, Germany

ABSTRACT The temperature-dependent ion conductance of OmpC, a major outer membrane channel of *Escherichia coli*, is predicted using all-atom molecular dynamics simulations and experimentally verified. To generalize previous results, OmpC is compared to its structural homolog OmpF at different KCl concentrations, pH values, and a broad temperature range. At low salt concentrations and up to room temperature, the molecular modeling predicts the experimental conductance accurately. At high salt concentrations above 1 M KCl and above room temperature, the simulations underestimate the conductance. Moreover, the temperature dependence of the channel conductance is different from that of the bulk, both in experiment and simulation, indicating a strong contribution of surface effects to the ion conductance. With respect to OmpC, subconductance levels can be observed in experiments only. Subconductance and gating levels can be clearly distinguished by their differences in conductance values and temperature-dependent behavior. With increasing temperature, the probability of a subconductance state to occur, increases, while the dwell time is decreased. The open probability, frequency, and dwell time of such states is largely pH- and KCl concentration-independent, while their amplitudes show a lower increase with increasing salt concentration than gating amplitudes. Voltage dependence of subconductance has been found to be negligible within the uncertainty of the measurements.

INTRODUCTION

The outer membrane of Gram-negative bacteria acts as barrier between the intracellular- and extracellular environment. Channel-forming membrane proteins called porins allow hydrophilic substrate permeation across this membrane. In addition to salt and carbohydrates permeation, these channels are also particularly interesting as a possible pathway for antibiotics to enter the cell. Among others, the bacterial adaption of the porin pattern is one akin to that of the resistance mechanisms (1). Therefore, it is essential to understand the relation between structure and mechanism in the transport through these porins. Ion and substrate permeation is governed by diffusion along the concentration gradients, electrical fields, or internal binding sites (2).

Escherichia coli produces two major porins, OmpF and OmpC (1,2). The OmpF-OmpC balance is highly regulated by different genetic control systems while OmpC, for example, is expressed at high osmotic stress. Both porins are trimers as shown by high-resolution x-ray crystallography (3,4). Each monomer is a 16-stranded hollow β-barrel. Both porins are structurally very similar: their sequences' identity is 60%, and 74% of the pore-lining residues are conserved (4). Both porins have a constriction zone near the middle of the channel, formed by the inward folded L3 loop. In this region, a strong transversal electric field is present due to the negatively charged residues on the L3 loop and the positive charges on the opposite side of the wall that are separated only by a short distance. The main charges in OmpF are the negatively charged residues D113 and E117 on L3, while the positive ones on the opposite channel wall are R42, R82, and R132. In OmpC the negative ones are D105 as well as E109, and the positive residues are R37, R74, and R124 (4). Furthermore, OmpC is slightly smaller than OmpF. Depending on the actual definition of the pore radius, it is reported to be 1.08 nm and 1.16 nm for OmpC and OmpF (5), respectively, or 1.0 nm and 1.1 nm (6). Both porins show a weak cation selectivity.

The main difference between OmpC and OmpF are in the ionizable residues resulting in a different potential in the constriction zone of the channels. Although structurally very similar, minor differences in these residues have a strong impact upon such kinetic properties as selectivity and channel conductance (2,4,6–8) and in voltage and spontaneous gating (6,7,9–11). Another noticeable difference is to be found at the outer pore wall that is formed by the extracellular loops in OmpC but not in OmpF (4). The outer loops (L1, L2, L4–L8), which are different in the two porins, might also be important with respect to voltage gating (6,7,12) or to pH sensitivity (12). The pore size as well as the specific binding sites evidently play an important role in selectivity (13) and in the uptake of antibiotics (1), polyamines (polyamine blocking) (6,7,14,15), or other molecules. The composition of the surrounding lipids, the porin plasticity, and lipopolysaccharides might also influence the behavior of the porin (6,7,16).

A molecular picture for the above-mentioned effects is still lacking. Ion conductance measurements readily allow the study of single channels, but the conductance represents an average over many ions. In contrast, the available

Submitted October 2, 2009, and accepted for publication January 13, 2010.

[△]István Biró and Soroosh Pezeshki contributed equally to this article.

*Correspondence: m.winterhalter@jacobs-university.de or u.kleinekathoefer@jacobs-university.de

Editor: Benoit Roux.

0006-3495/10/05/1830/10 $2.00
doi: 10.1016/j.bpj.2010.01.026

high-resolution x-ray crystal structures (17,4,18) provide a static view with atomic resolution and at the same time allow the molecular modeling of the corresponding pores. In previous molecular dynamics (MD) simulations, the ion permeation through an OmpF monomer were studied (19). Im and Roux (20,21) used continuum models (Poisson-Nernst-Planck theory), grand canonical Monte Carlo, Brownian dynamics, and MD techniques to simulate OmpF trimers embedded in a membrane. The recent improvements in computational performance and the development of new algorithms allowed large-scale MD simulations of biological and artificial pores (22–28). Importantly, it became possible to simulate ion conduction directly using applied field MD simulations (25–28) although it is still under debate how to apply the voltage most accurately and efficiently (29–31). This technique was recently also applied to OmpF (32,33), and good agreement with experiment was obtained. The advantage of the MD simulations are their atomic level details, which help to elucidate more details about the involved transport mechanisms including, e.g., ion paths and ion pair probabilities.

Here we investigate OmpC because of its high homology to OmpF, which, combined with the differences in its physical and transport properties may bring us closer to understanding the basic mechanisms of pore kinetics and transport. Furthermore, OmpF and OmpC are the most abundant pores in the outer membrane of Gram-negative entero-bacteria and thus represent a major pathway for substrate transport. This pore is an excellent choice for studies of the temperature dependence, as its gene expression is favored at relatively high temperatures (34). In addition, low-temperature environments have been shown to alter the translocation properties (35). This shows that the detailed knowledge of the involved transport mechanisms and their temperature dependence will also help to make translocation events more predictable and experiments easier to interpret.

In addition to the conductance through open pores, different levels of conductance (the so-called subconductance states and gating) can be observed. The terminology is used differently in various studies but in this article, ''gating'' refers to single monomeric closures (conductance drop by one-third of the full trimer conductance), while ''subconductance'' is the term we use for conductance drops smaller than drops resulting from single monomer closures. Although gating is often reported, only few articles mention subconductance states (36–38). Nevertheless, the molecular mechanisms for gating and subconductance are so far unclear and/or under debate.

The main goal of this article is to elucidate the quality of computer modeling by comparing two structural homologs (OmpC and OmpF). Particularly we compare the theoretical temperature-dependent ion conductance with the experimentally measured one. In addition to the pore conductance, we also address the kinetic side of this behavior through the experimental analysis of the subconductance. A direct simulation of the kinetics of subconductance states is not possible because of the limited time accessible in MD simulations. Nevertheless, the thermal fluctuations in the simulations are analyzed.

This article is organized as follows: Subsequent to the details of the experimental and computational setups, the results for conductance, free energy profiles, and subconductance states are reported. Thereafter the experimental as well as theoretical outcomes are discussed and an outlook is given.

MATERIALS AND METHODS

Experimental setup and chemicals

The details of the extraction and purification of OmpC are given in the Supporting Material. The experimental setup has been described previously (32,39–41), to which no modifications were necessary in this case. Thus, here only a few relevant details are given.

Two plastic buffer-filled compartments are separated by a 25-μm-thick Teflon film (Goodfellow, Cambridge, UK), which has a hole of ~60-μm diameter. The area around the hole is prepainted with 1% squalene solution and a bilayer is formed over the hole using 1,2-diphytanoyl-*sn*-glycero-3-phosphatidylcholine (DPhPC; Avanti Polar Lipids, Alabaster, AL), according to the Montal-Mueller method (42). DPhPC has no detectable gel-to-liquid-crystalline phase transition over a large temperature range (−120°C to +120°C), and thus allows our performing experiments at all temperatures studied here (43). Using two Ag/AgCl electrodes (World Precision Instruments, Sarasota, FL), a potential difference is applied across the bilayer. Thus, the ions permeating through an OmpC pore inserted in the bilayer give rise to a current that is amplified (using an Axopatch 200B amplifier, with headstage model No. CV 203BU; Axon CNS Instruments, Foster City, CA), digitized (Digidata 1440A digitizer; Axon CNS Instruments), recorded (using Clampex software version 10.0 and 10.2; Molecular Devices, Eugene, OR), and evaluated (using Clampex software, Vers. 10.0 and 10.2; Molecular Devices). During the measurements, the temperature of the setup is actively controlled (using a model No. HE-BLM with an HCC-100A heating-cooling bath temperature controller; Dagan, Minneapolis, MN).

The protein was always added to the *cis* side, at which the potential was 0 V while the applied *trans*-membrane voltage was in the range of −100 to 100 mV during most of the measurements. In a few additional experiments performed in a voltage range of −250 to 250 mV, the current-voltage relationship was shown to be linear. Starting at ~250 mV, the pore shows strong gating and quickly closes fully. The remaining leak current, after all three monomers are closed in this way, is small compared to the open pore current, and thus such leaks are neglected in this study. Therefore, the conductance is directly obtained as measured current over applied voltage. Furthermore, in this investigation all current recordings have been performed using a 5-kHz low-pass Bessel filter. In addition, all buffers used in the measurements were prepared using double-distilled water, to which KCl (AppliChem, Darmstadt, Germany) was added in the desired amount and additionally contained 10 mM potassium-phosphate (H_2KO_4P and HK_2O_4P; Fluka, Buchs, Switzerland). Moreover, the desired pH values were achieved by using different ratios of acidic and basic potassium-phosphate. In this way a pH range from ~4.4 to ~8.8 can be covered without the addition of other chemicals. This is the pH range studied here. During some measurements, mineral oil (paraffin oil light; AppliChem) was added on top of the buffer to minimize evaporation at high temperatures, while during others the buffer containing cuvette entrance was covered for the same purpose. Generally, oil was used to achieve this goal, as this technique is easier to implement. To rule out artifacts occasioned by the oil on the subconductance, measurements that are more technically difficult (in which no oil was added but the cuvette

entrance was covered) were also carried out. Thus, we could show that oil on top of the buffer does not have a significant effect on subconductance.

Setup of the simulations

In the following, we briefly describe the simulation setup. As a starting structure, the x-ray structure of the OmpC pore, as published by Baslé et al. (4) (PDB ID: 2J1N), was employed. All residues of the protein are assumed to stay in their normal protonation state. The OmpC trimer was embedded into POPE lipid bilayer and TIP3P water and KCl ions were added to obtain the required salt concentration and to neutralize the system. A hexagonal simulation box was used with 63 Å side length and a thickness of 80 Å, leading to a total atom number of ~88,000. After a short minimization, the system is equilibrated in an NpT ensemble for 1 ns. During the actual production runs, an NVT ensemble was also employed. Langevin damping was applied on the heavy lipid atoms with a damping constant of 1.0 ps^{-1}. Furthermore, periodic boundary conditions were used, together with the particle-mesh Ewald method, for the calculation of the electrostatics.

The MD simulations were performed using NAMD 2.6 (44) together with the CHARMM27 force field (45). The ionic conductance through the pore was determined by following the general method described in Aksimentiev and Schulten (25). To be able to count more ions per time units and in this way obtain a better statistics, a voltage of 1.0 V was applied in the simulations. In experiments, a linear IV curve is observed (33); thus, the high-voltage difference between experiment and simulation is assumed not to introduce a major deviation in the simulation results. Because of the relatively high error bars in the simulations (especially for low voltages), a reliable current-voltage curve is hard to obtain from the simulations. We therefore rely on the experimental curve. Each current value was calculated from the motion of the ions in a 10-ns trajectory. In these, an homogeneous external field E in z direction was applied proportional to the voltage V,

$$E = V/L_z,$$

with the system length in z direction L_z. The field was applied using the built-in function of NAMD 2.6 (44). Because the ions in the water are free to move and periodic boundary conditions are assumed, the rearrangement of the ions leads to a highly nonlinear electric field. Further simulation details are presented in Pezeshki et al. (33).

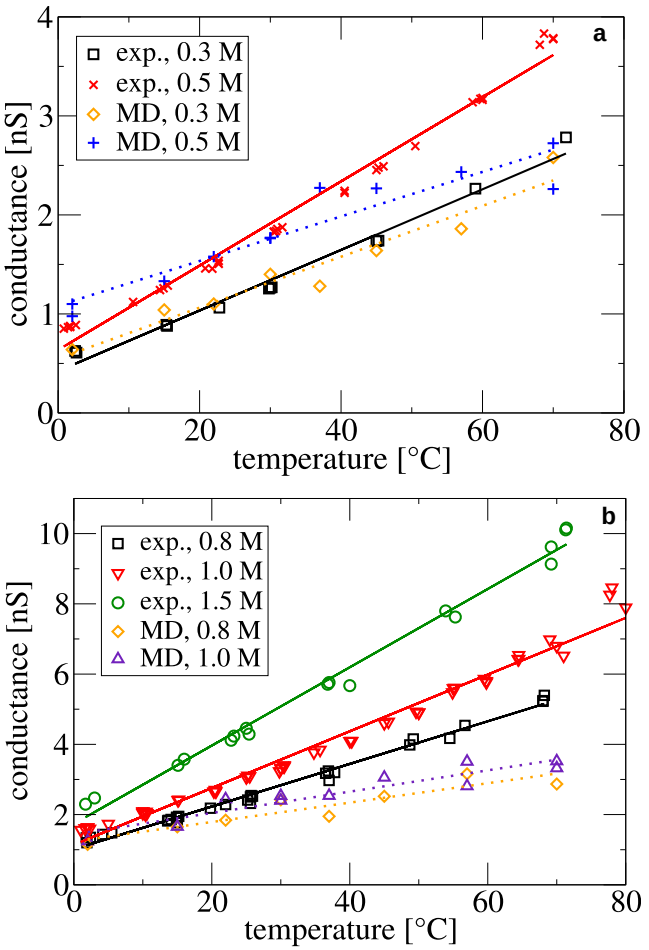

FIGURE 1 Temperature dependence of OmpC conductance for different salt concentrations in experiment and simulation. To guide the eye, also the linear interpolations are shown. (*a*) Experimental and computational results in rather good agreement for low salt concentrations. (*b*) Results for high KCl concentrations with increasing deviations between theory and experiment. The pH value of the buffer was 7.5.

RESULTS

Conductance in experiment and simulations

As first results, we report the measurements of the OmpC conductance as a function of temperature for various KCl concentrations and compare the results with MD simulations. In Fig. 1, the conductance is shown for four different KCl molarities and, as expected, the pore conductance increases linearly with temperature and with salt concentration.

At low salt concentrations and low temperatures, the simulations accurately describe the experimental data. In Fig. 1 *a*, it is shown that for 0.3 M the simulation and the experimental conductance agree nicely. For 0.5 M, the slope of the temperature dependence of the conductance is the same for the simulation and experiment in the temperature range from 15 to 37°C. The overall slopes are different as the theoretical and experimental conductances differ quite a bit at higher temperatures. At higher salt concentrations and above room temperature, the modeling starts to deviate. Deviation between experimental values and simulations is already observed for the bulk conductivity, i.e., a simple system of a water box with ions, as has been shown in Pezeshki et al. (33). Because this deviation becomes large for salt concentrations above 1 M, no simulations were performed that paralleled the 1.5 M experiments. Nevertheless, it is interesting to note that the agreement between modeling and measurements is significantly better for OmpC compared to OmpF (32,33), for the entire temperature and salt concentration range, as shown in Fig. S1 in the Supporting Material.

Furthermore, the experimentally observed increase of the conductance with the salt concentration shows no saturation effects at the studied concentrations. Thus, doubling the salt concentration from 0.5 M to 1.0 M leads to an almost doubled conductance, but in OmpF, doubling from 0.5 M to 1.0 M leads to an increase of less than two times. Concerning a pH variation within the range of 4.4 and 8.8, no significant change has been observed (data not shown).

To elucidate the effect of the channel, we separate the temperature effect of the bulk conductivity and the remaining effect of the channel. To this end, we normalize the channel conductance by using the ratio of the pore conductance over the bulk conductivity. In our measurements, this ratio depends less on the salt concentration for OmpC than for OmpF, as shown in Fig. S2. Although for OmpF a change with different salt concentrations is observed (32), for OmpC there is almost no change for 0.5 and 1.0 M. This is in accordance with the concentration dependence of the conductance of OmpC and OmpF that we mentioned above. The results lead to the conclusion that the ion transport is significantly different for both pores, OmpC and OmpF, which is caused by minor electrostatic differences in the structure of the pore lumen.

The same tendency is seen in the simulations. On average, OmpC is found to have a smaller ratio of the pore conductance over the bulk conductivity, but the difference between the pores seems less pronounced compared to experiment. Trends in the data show a increase of the ratio with increasing temperature. In Pezeshki et al. (33), an error of $\pm 20\%$ was estimated for the OmpF calculations and similar error will also hold for the OmpC calculations. Therefore, more-precise conclusions from the simulations are impossible at this time.

Ion densities, pathways, and free energy profile

In Fig. 2, the pore area based on simulations at 37°C is shown as a function of the position along the channel axis for OmpF and OmpC. The OmpF profile is in agreement with the one reported earlier by Im and Roux (20). One can see that the constriction zone (i.e., the narrowest part of the channel) for OmpC is roughly 10 Å long, whereas for OmpF its length is only ~5 Å. Responsible for the longer constriction zone in OmpC might be the positively charged residue K317, which attracts the negatively charged residues on the L3 loop E109 and D113, as shown in Fig. S3. The L3 loop of OmpF is folded less into the volume of the pore partly because of the missing positively charged residue corresponding to K317. More details on the difference between the OmpF and OmpC constriction zone structures are given in the Supporting Material. The additional negatively charged residue D113 and the less-exposed positive charges explain the larger cation selectivity of OmpC compared to OmpF.

To elucidate the behavior of the ions within the pore, we extracted from the simulations the number of ions within the OmpC channels within 3 Å of the pore surface compared to all ions in the pore. As shown in Fig. 3 *a*, ~50% of all ions are found in this region, confirming the importance of surface effects. This claim is supported by the experimental pore conductance showing no apparent saturation in a concentration range from 0.3 M to 1.5 M (data not shown). Comparing the ratio of ions at the surface found in OmpC with that in OmpF, one observes a significantly higher ratio

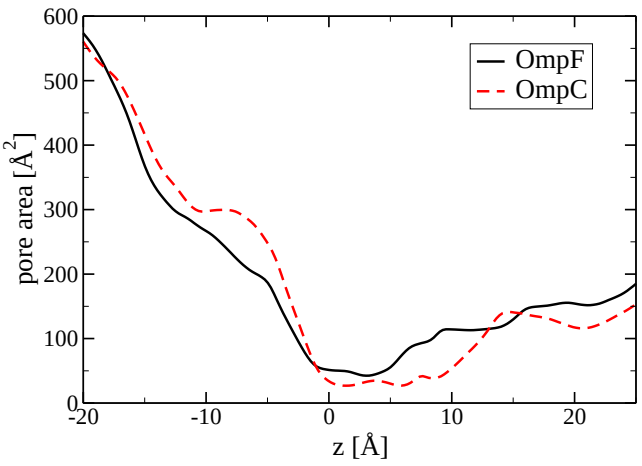

FIGURE 2 Cross-section area of the OmpC and the OmpF pore as a function of the channel position z averaged over 10-ns trajectories. The β-barrel extends from z values of -17 to 15 Å.

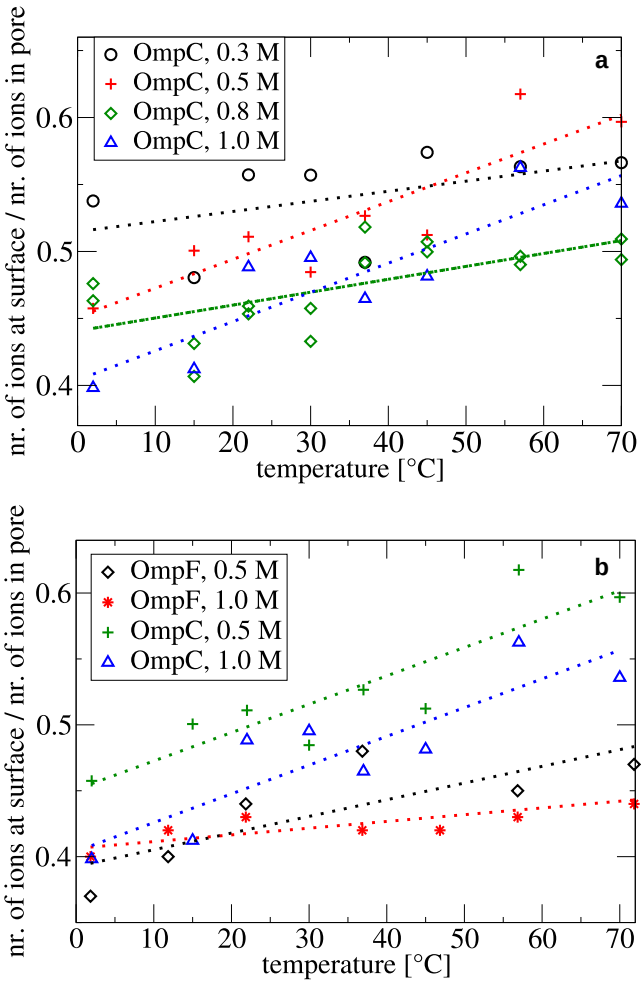

FIGURE 3 Calculated number of ions within 3 Å distance from the surface relative to the total number of ions. (*a*) Results are shown for various salt concentration in OmpC. (*b*) Comparison between OmpC and OmpF at 0.5 M KCl and 1 M KCl.

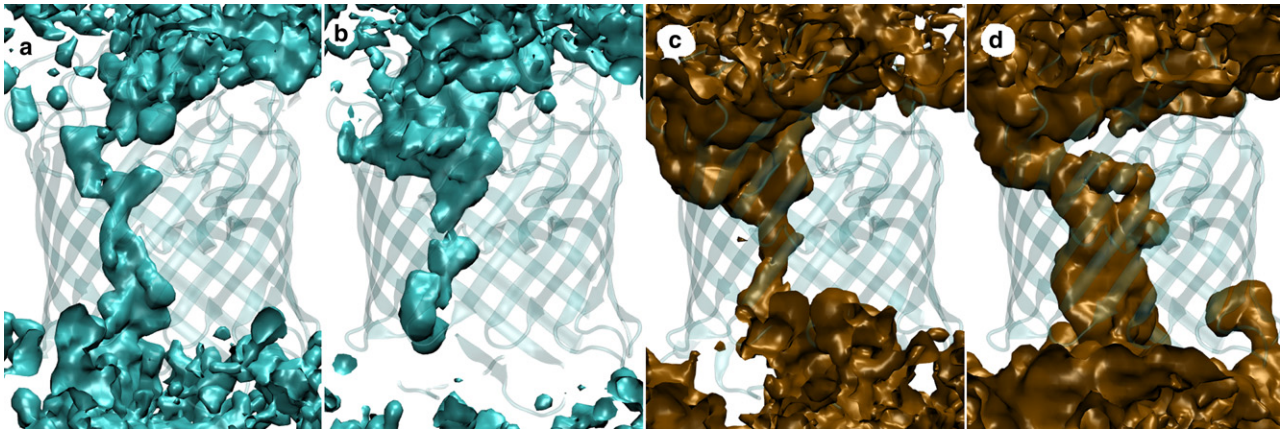

FIGURE 4 Isosurfaces of ion density for simulations with 22°C at 0.5 M KCl. (*a*) Cl^- density in OmpF, (*b*) Cl^- density in OmpC, (*c*) K^+ density in OmpF, and (*d*) K^+ density in OmpC. All isosurfaces represent the same density value. Figures generated using VMD (50).

for the former pore, as seen in Fig. 3 *b*. The ratios correspond to the average ratio of the volume within 3 Å from the pore walls to total volume. For these calculations, only the ions in the β-barrel region were considered, i.e., ions within $z > -17$ Å and $z < 16$ Å. For both pores, the ratio of ions at the surface over all ions is smaller for higher salt concentrations, and it grows with temperature. The temperature dependence is slightly stronger in OmpC than in OmpF; however, this lies within the error range of our simulations.

In connection with a recent study of ionic current through silica nanopores (27), we mention that, in said study, the system has ion-binding spots to which the ions do bind for some time, i.e., in some situations for several nanoseconds. This, in turn, has, of course, significant effects on the electrostatics in the channel and therefore on the conductance.

Further analyzing the MD simulation results reveals that the ratio of the potassium current over the chloride current is higher for OmpC than for OmpF; the ratios for 1 M KCl at room temperature are 2.9 and 1.2 (33), respectively. For OmpF, the current ratios were transformed into selectivities that can be determined using the reversal potential. For this, a fixed proportionality factor of 3.5:1.2 between selectivity and current ratio was assumed as independent of the actual mutation under consideration (33). Assuming the same factor for OmpC, a selectivity of 8.5 is estimated from the simulations. The corresponding experimental values vary from 5.8 (4) to 26 (6,2), i.e., certainly larger than that of OmpF. In addition, the simulations give information about the pathways of the ions through the channel. In Fig. 4 the isosurfaces of the ion density in OmpF and OmpC are shown. As already seen for OmpF (21,33), the main pathways of the positive and negative ions show a screwlike pattern and do not intersect. The graphs show that the chloride ion density is very small at the periplasmic entrance of the OmpC pore. On the other hand, the potassium density is higher in OmpC than in the OmpF pore. It is interesting to note that although the densities differ in details, both pores lead to relatively similar pathways of the ions.

The free energy profile allows us to estimate the work needed to translocate an ion through the porin. It shows where the main transport barriers exist but also where the wells, which attract ions, are located. For multiion systems, the one-dimensional profiles are calculated as (21)

$$W_\alpha(z) = -k_B T \ln\left(\rho_\alpha(z)/\rho_\alpha^{\text{bulk}}\right), \quad (1)$$

with the Boltzmann factor k_B, the ion density $\rho_\alpha(z)$ of ion type α at position z, and the bulk density $\rho_\alpha^{\text{bulk}}$. The obtained energy profiles reveal the change of the free energy of the ions in dependence of the z position along the channel axis. The free energy in the bulk is used as reference energy. Previously, Im and Roux (21) calculated the free energy profile based on the Brownian dynamics approach. Here, the all-atom MD simulations provide more atomic details, but with the drawback of a poor statistic, i.e., larger possible errors. The results for OmpC and OmpF are displayed in Fig. 5. It is interesting to note that single ions are trapped next to charged residues in the pores. Such events are long-lived and have, partially based on the poor statistics, a strong influence on the outcome of the calculation. The free energy profiles reveal both energy barriers for the chloride ions and wells for potassium ions. The attractive region for the K^+ ions is between energy barriers—smaller ones for OmpC, and a high energy barrier for OmpF. These formations constitute the reason for the higher potassium current through OmpC. The attraction is caused by negative charges in the constriction zone that trap positive K^+ ions. Although the barrier in the chloride profile is wider for OmpF, OmpC has a higher peak, at z values of ~15 Å, that lead to low chloride conductance.

Subconductance

In this part of the article, we will focus on the kinetic temperature-dependent behavior of the OmpC pore. Experimental observations have shown the presence of subconductance states for OmpC. Gating between the levels occurs on

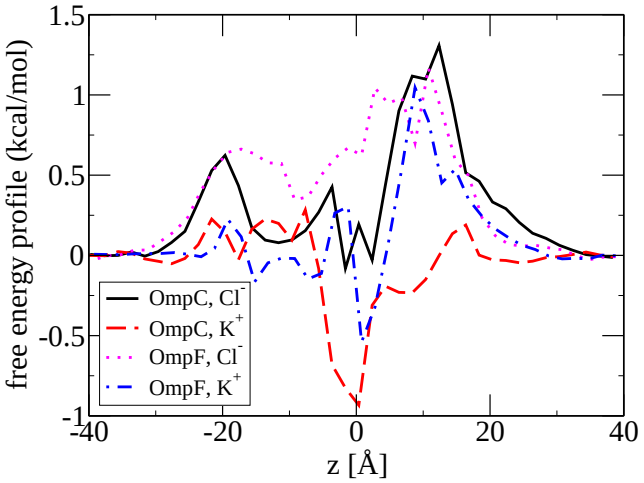

FIGURE 5 Free energy profiles for OmpC and OmpF for simulations with 0.5 M KCl at 22°C with a bin size of 2 Å along the channel axis. The energy values are compared to the bulk free energy ($z < -25$ Å and $z > 25$ Å).

a millisecond-to-second timescale, rendering MD modeling, at the time of this article, impossible. One needs to note that subconductance states clearly differ from gating, as the former ones are much smaller in amplitude and occur at low voltages as well. In our case, measurements were performed at 50-mV applied voltage, whereas gating is observed at >200–250 mV. Such subconductance states are presented in Fig. 6 and in the following a more detailed

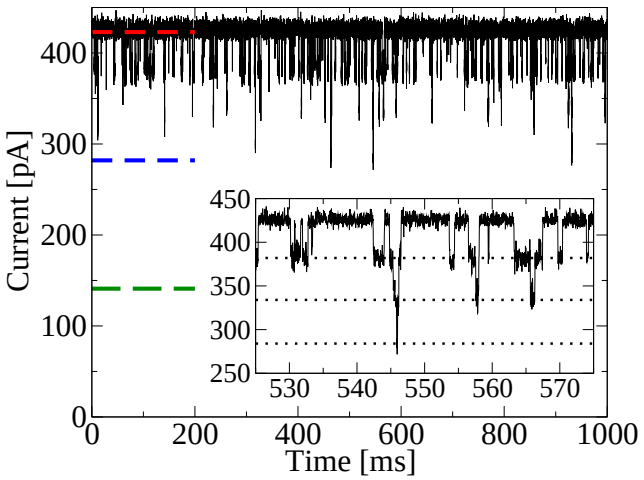

FIGURE 6 Current recording of a single OmpC pore at 78°C, in 1 M KCl at an applied voltage of 50 mV. The main panel shows 1 s from a recording. The current baseline for a fully closed pore is 0 pA, whereas the dashed horizontal lines indicate current levels of one, two, and three open monomers, respectively. Subconductance states are short, partial closings, which appear as downward spikes from the open pore-current level. (*Inset*) Magnified area of the above trace. Dotted lines show the current drops resulted by one, two, and three simultaneous subconductance events, respectively. One subconductance drop is significantly smaller than a monomeric closure. Subconductance events can overlap, resulting in a larger current drop; however, no greater than three such closures are observed simultaneously for one porin. This suggests a maximum of one closure level for each monomer.

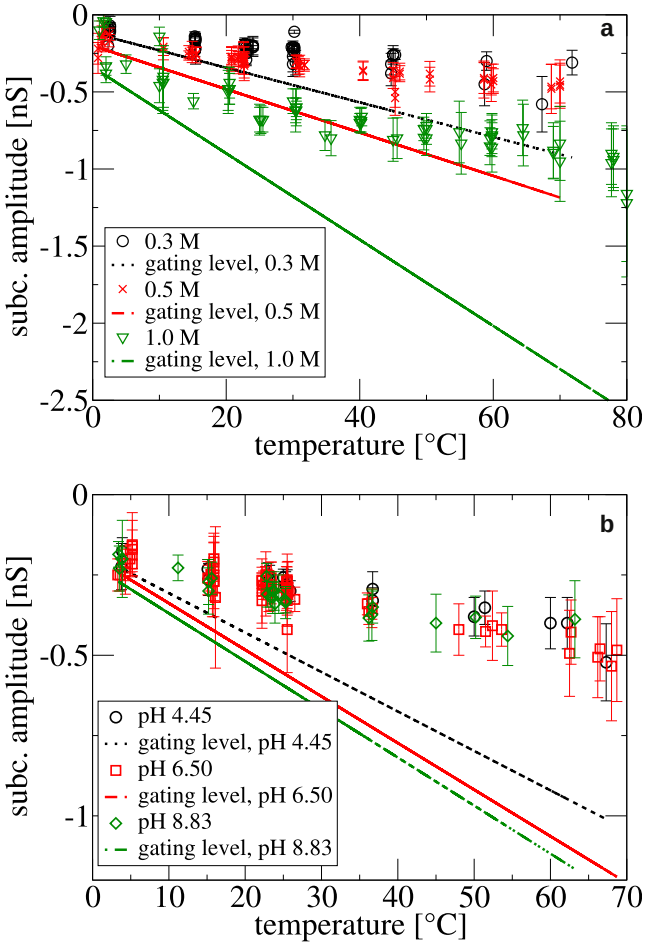

FIGURE 7 Temperature dependence of the subconductance amplitude (*a*) for different salt concentrations and (*b*) for different pH values. Subconductance amplitudes are shown with symbols and their error bars, while the expected levels for gating are represented by lines.

analysis of these states is presented. To avoid confusion, here we state the definition of certain quantities we will use for the characterization of such events. ''Subconductance frequency'' is the number of subconductance events over measurement time for one pore, and ''open probability'' represents the time spent by the pore in the subconductance state over the total measurement time. The ''dwell time'' is the average time of one subconductance state; and the ''subconductance amplitude'' is the difference between the conductance of the pore in subconductance state (lower state) and that of the open pore (higher state).

First, we studied the amplitude of the subconductance (closings). The results, displayed in Fig. 7, clearly indicate subconductance values. These states not only have smaller values of conductance reduction than the monomeric conductance, but also a much weaker temperature dependence—and the reductions in the current increase with the salt concentration. We also found no apparent dependence of these levels on the pH value in the pH range from 4.4 to 8.8. The results together with the errors bars are shown in Fig. 7.

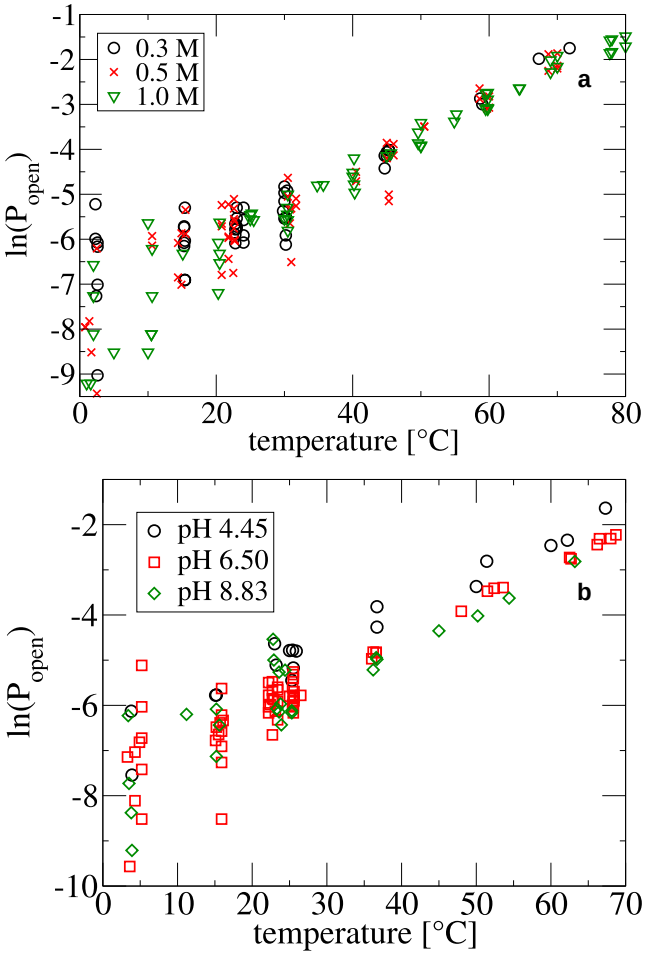

FIGURE 8 Temperature dependence of the subconductance open probability (i.e., the probability to find the pore in a subconductance state) (*a*) for different salt concentrations and (*b*) for different pH values. The error values are higher at low temperatures due to poor statistics.

Even more surprising was our finding regarding the temperature dependence of the frequency and the open probability of the subconductance states: both of these show an exponential increase. They are even independent from buffer pH value and salt concentration. These results are clearly shown in Fig. 8 and Fig. S4. In addition, the dwell time of the subconductance states is independent from the salt concentration and pH value but decreases exponentially with increasing temperature, as shown in Fig. S5. At this point one has to state that the relatively large error bars and deviations at low temperatures make a clear analysis difficult. Thus, we only point out the type of these dependencies and suggest further studies be undertaken for improved explanations.

Within a pH range of 6.5–7.5, a temperature range of 0–70°C, and a concentration range of 0.3 M–1.0 M, we counted the occurrence of higher subconductance frequency and open probability values, for the cases of negative- and positive-applied voltage, respectively. We found a larger subconductance frequency and open probability for positive-applied voltages in 17 (for the frequency) and 11 (for the open probability) measurements (out of a total of 64), respectively. For negative voltage, these numbers were 47 and 50, respectively. Thus, negative-applied voltage seems to result in a larger probability for the occurrence of subconductance. However, as these differences are very small (in our experiments within the error range), these can be neglected, compared to the significantly stronger influence of temperature.

As mentioned above, the direct simulation of gating and subconductance is currently unfeasible. Nevertheless, one can analyze the fluctuations of different residues during several MD trajectories. This reveals that the extracellular loops L4, L5, and L7, the periplasmic turns T1 and T4, and the inner loop L3, have the largest fluctuations for OmpC. Typical fluctuation patterns of the residues are shown in Fig. S3. Other simulations have shown other peak heights, but the same positions (e.g., the residues with the largest fluctuations are the same in all simulations). Concerning the comparison between OmpC and OmpF, the L4 loop fluctuates considerably more in OmpC—independent of salt concentration and temperature. A look at the sequences reveals that, in OmpC, the L4 loop has 14 residues more than in OmpF and is, therefore, much longer (4). This extended length could be a reason for larger fluctuations and also for the occurrence of the subconductance states. In OmpF, the high fluctuation of the L6 loop was also observed by others (20,46).

DISCUSSION AND OUTLOOK

Conductance in experiment and MD

As shown in the previous section, the agreement between measured and simulated conductance results is very encouraging, although there is certainly room for improvement, especially for higher salt concentrations and temperatures. The deviations can partially be explained by the missing temperature dependence of force fields, optimized only at room temperature, and their very bad performance for high ionic concentrations. As of the time of this writing, there are no standard force fields for proteins and lipids that are parameterized in a temperature-dependent fashion and that are well suited for being used at higher temperatures. These deficiencies were already analyzed for the simple case of bulk conductivity (33), and are expected to be similar in this work. In a previous study on OmpF, we have estimated an error of 20% for the MD simulations (33) and similar error bars need to be taken into account for the MD results presented here.

Because OmpC and OmpF are rather similar, mutation studies that involve the deletion of a charged residue in one pore and the deletion of its equivalent residue in the other one might be presented as interesting approaches for both the experimental and modeling studies of conductance

and ion pathway changes. Furthermore, despite the homology of OmpC and OmpF, not all charged residues have equivalent residues in the other porin. Mutating these residues, e.g., in OmpC, will show their influence on conductance and selectivity. One basic question that could be solved this way is whether the number and the position of the charged residues is responsible for the different behavior of OmpC and OmpF. Residues that are exposed to the pore lumen are more favorable for mutations in this respect.

In this article, the relatively small changes in OmpC conductance with changing pH values in the range between 4.4 and 8.8, as obtained in the experiments, are in good agreement with a study performed on OmpF (47). The latter study also shows a conductance plateau between these pH values and strong changes otherwise. Extending the conductance studies of OmpC to more extreme pH values is thus desired not only for a better comparison but more importantly for the possibility of getting a detailed insight into the behavior of the protonation states inside the pore.

One way to approach the task described immediately above would be to do the above-proposed conductance measurements (on a large scale of buffer pH values) for OmpC as has been done for OmpF (47). Connecting the differences in the conductance properties with structural deviations and simultaneously modifying protonation states in MD simulations, to obtain the best agreement with these measurements, could result in calibration of the protonation in the pore model. On the theoretical side, e.g., it was suggested by Varma et al. (46) to calculate the intrinsic pKa of a titrable site assuming nontitratability of all other sites and then calculate the effect of the other titrable sites. Although the issue of protonation states is quite important for a detailed understanding of ion transport, it needs further work.

Subconductance

Subconductance states similar to those presented here have been observed for other pores as well. Under particular conditions, OmpA has been shown to have two open states with different conductance values, between which the dominant one is being determined by the temperature (36), while OmpG traces have also shown conductance flickering and gating, eliminated by mutations (38). The presence of subconductance in OmpF is debated: it has been confirmed in some cases ((37) and Roland Benz, Jacobs University Bremen, personal communication, 2009), whereas other studies have shown an absence of subconductance (Catalin Chimerel, Jacobs University Bremen, personal communication, 2009). Most literature sources do not even mention such observations for OmpF or for OmpC. Subconductance in OmpC was reported in a few cases only, and not fully analyzed ((9,10,38) and Roland Benz, Jacobs University Bremen, personal communication, 2009).

Thus, more studies in this direction are needed to resolve this issue. Furthermore, it is very important to extensively verify extraction and purification protocols to exclude possible functional changes of the pores caused by these techniques. Because of this, caution has to be taken when interpreting this study as well as previous studies.

The results presented above regarding the subconductance states of OmpC are quite intriguing as they bring us closer to the understanding of its behavior. As shown, the subconductance frequency and open probability not only increase exponentially with temperature and are indifferent to salt concentration or pH value of the buffer, but at the same time seem to be only slightly influenced by the applied voltage. However, as the error bars are reasonably large, an increased number of measurements under different conditions is required to investigate the voltage dependence of subconductance in more detail. All these results lead us to the hypothesis that subconductance is not governed by electrostatics but rather by short-lived and repeated conformational changes of the pore. This assumption seems to be validated by the subconductance amplitudes, showing no dependence on the pH value but, instead, a slight increase with increasing salt concentration.

Furthermore, we believe the subconductance gating to be governed by fluctuations of certain residues, causing the conformational changes that lead to subconductance. The reason for this assumption is manifold. First, we showed an exponential increase of frequency and open probability with temperature which is consistent with increasing residue fluctuation caused by thermal excitations. Another observation pointing in this direction is the exponentially decreasing dwell time with temperature (i.e., a decrease of the time length of single subconductance events), suggesting faster kinetics. However, the porin remains stable and no denaturation occurs after exposure of the pore to high temperatures and while the buffer temperature is reduced. During these processes, conductance and kinetic properties are reproduced within rather small deviations caused by evaporation (minimized but not completely eliminated by oil).

In the MD simulations, strong fluctuations, especially in the L4 loop of OmpC, were observed. These findings are, however, insufficient for a complete explanation of the subconductance but might be an important hint for its operating. The results of this study will be used for the creation of OmpC mutants, preferably starting with a partial deletion or fixation of the L4 loop to verify its importance in subconductance. So far, one cannot exclude other reasons for the appearance of subconductance states such as the presence of lipopolysaccharides, the plasticity of the pore (16), or other external loops, which have been shown to be more flexible than believed from the crystal structure (48). Note also that loop L3 is believed to be involved (37). Therefore, to exclude any effect of the extraction and purification methods employed, we propose another set of measurements with porins extracted and purified using slightly different protocols.

Investigations in a large pH range for OmpC are also motivated by the observed conductance fluctuations in OmpF,

showing growth in frequency at very high or very low pH values, and having a frequency minima at more moderate pH values (47). These fluctuations appear to be extremely similar to the subconductance states observed to increase exponentially with temperature; however, they are rather pH-independent within the error range in our present work for OmpC. In regard to this similarity, it would be interesting to compare these two effects—i.e., pH and temperature dependence.

In this contribution we focused on the transport of ions through two different but structurally similar porins, OmpF and OmpC, in experiments and molecular simulations. Not only the results but also the questions presented above might well contribute to the understanding of permeation of substrate molecules across the channel. For this purpose, studies of the transport of certain antibiotics and polyamines through OmpC are currently in progress. These can then be compared to existing studies of transport through OmpF (1,49).

SUPPORTING MATERIAL

Six figures are available at http://www.biophysj.org/biophysj/supplemental/S0006-3495(10)00159-1.

We express our gratitude to Prof. Dr. Roland Benz, Mahendran Kozhinjampara, and Catalin Chimerel for fruitful discussions, and to Robert Schulz and Enrico Spiga for their help.

We acknowledge financial support through grant No. MRTN-CT-2005-019335 (Translocation) and the Deutsche Forschungsgemeinschaft.

REFERENCES

1. Pagès, J. M., C. E. James, and M. Winterhalter. 2008. The porin and the permeating antibiotic: a selective diffusion barrier in Gram-negative bacteria. *Nat. Rev. Microbiol.* 6:893–903.
2. Benz, R., and K. Bauer. 1988. Permeation of hydrophilic molecules through the outer membrane of Gram-negative bacteria. Review on bacterial porins. *Eur. J. Biochem.* 176:1–19.
3. Cowan, S. W., R. M. Garavito, …, J. P. Rosenbusch. 1995. The structure of OmpF porin in a tetragonal crystal form. *Structure*. 3: 1041–1050.
4. Baslé, A., G. Rummel, …, T. Schirmer. 2006. Crystal structure of osmoporin OmpC from *E. coli* at 2.0 Å. *J. Mol. Biol.* 362:933–942.
5. Seltmann, G., and O. Holst. 2002. The Bacterial Cell Wall. Springer, Berlin.
6. Benz, R., A. Schmid, and R. E. Hancock. 1985. Ion selectivity of Gram-negative bacterial porins. *J. Bacteriol.* 162:722–727.
7. Delcour, A. H. 2003. Solute uptake through general porins. *Front. Biosci.* 8:d1055–d1071.
8. Danelon, C., A. Suenaga, …, I. Yamato. 2003. Molecular origin of the cation selectivity in OmpF porin: single channel conductances vs. free energy calculation. *Biophys. Chem.* 104:591–603.
9. Liu, N., and A. H. Delcour. 1998. The spontaneous gating activity of OmpC porin is affected by mutations of a putative hydrogen bond network or of a salt bridge between the L3 loop and the barrel. *Protein Eng.* 11:797–802.
10. Liu, N., H. Samartzidou, …, A. H. Delcour. 2000. Effects of pore mutations and permeant ion concentration on the spontaneous gating activity of OmpC porin. *Protein Eng.* 13:491–500.
11. Mobasheri, H., and E. J. Lea. 2002. Biophysics of gating phenomena in voltage-dependent OmpC mutant porin channels (R74C and R37C) of *Escherichia coli* outer membranes. *Eur. Biophys. J.* 31:389–399.
12. Baslé, A., R. Qutub, …, A. H. Delcour. 2004. Deletions of single extracellular loops affect pH sensitivity, but not voltage dependence, of the *Escherichia coli* porin OmpF. *Protein Eng. Des. Sel.* 17:665–672.
13. Vrouenraets, M., J. Wierenga, …, H. Miedema. 2006. Chemical modification of the bacterial porin OmpF: gain of selectivity by volume reduction. *Biophys. J.* 90:1202–1211.
14. Kwon, D. H., and C. D. Lu. 2007. Polyamine effects on antibiotic susceptibility in bacteria. *Antimicrob. Agents Chemother.* 51:2070–2077.
15. Iyer, R., Z. Wu, …, A. H. Delcour. 2000. Molecular basis for the polyamine-OmpF porin interactions: inhibitor and mutant studies. *J. Mol. Biol.* 297:933–945.
16. Buehler, L. K., S. Kusumoto, …, J. P. Rosenbusch. 1991. Plasticity of *Escherichia coli* porin channels. Dependence of their conductance on strain and lipid environment. *J. Biol. Chem.* 266:24446–24450.
17. Cowan, S. W., T. Schirmer, …, J. P. Rosenbusch. 1992. Crystal structures explain functional properties of two *E. coli* porins. *Nature.* 358:727–733.
18. Yamashita, E., M. V. Zhalnina, …, W. A. Cramer. 2008. Crystal structures of the OmpF porin: function in a colicin translocon. *EMBO J.* 27:2171–2180.
19. Suenaga, A., Y. Komeiji, …, I. Yamato. 1998. Computational observation of an ion permeation through a channel protein. *Biosci. Rep.* 18:39–48.
20. Im, W., and B. Roux. 2002. Ions and counterions in a biological channel: a molecular dynamics simulation of OmpF porin from *Escherichia coli* in an explicit membrane with 1 M KCl aqueous salt solution. *J. Mol. Biol.* 319:1177–1197.
21. Im, W., and B. Roux. 2002. Ion permeation and selectivity of OmpF porin: a theoretical study based on molecular dynamics, Brownian dynamics, and continuum electrodiffusion theory. *J. Mol. Biol.* 322:851–869.
22. Bond, P. J., and M. S. Sansom. 2004. The simulation approach to bacterial outer membrane proteins. *Mol. Membr. Biol.* 21:151–161.
23. Roux, B., T. Allen, …, W. Im. 2004. Theoretical and computational models of biological ion channels. *Q. Rev. Biophys.* 37:15–103.
24. Tieleman, D. P. 2006. Computer simulations of transport through membranes: passive diffusion, pores, channels and transporters. *Clin. Exp. Pharmacol. Physiol.* 33:893–903.
25. Aksimentiev, A., and K. Schulten. 2005. Imaging α-hemolysin with molecular dynamics: ionic conductance, osmotic permeability, and the electrostatic potential map. *Biophys. J.* 88:3745–3761.
26. Sotomayor, M., V. Vásquez, …, K. Schulten. 2007. Ion conduction through MscS as determined by electrophysiology and simulation. *Biophys. J.* 92:886–902.
27. Cruz-Chu, E. R., A. Aksimentiev, and K. Schulten. 2009. Ionic current rectification through silica nanopores. *J. Phys. Chem. C*. 113:1850–1862.
28. Cruz-Chu, E. R., T. Ritz, …, K. Schulten. 2009. Molecular control of ionic conduction in polymer nanopores. *Faraday Discuss.* 143:47–62.
29. Delemotte, L., F. Dehez, …, M. Tarek. 2008. Modeling membranes under a transmembrane potential. *J. Phys. Chem. B*. 112:5547–5550.
30. Böckmann, R. A., B. L. de Groot, …, H. Grubmüller. 2008. Kinetics, statistics, and energetics of lipid membrane electroporation studied by molecular dynamics simulations. *Biophys. J.* 95:1837–1850.
31. Roux, B. 2008. The membrane potential and its representation by a constant electric field in computer simulations. *Biophys. J.* 95: 4205–4216.
32. Chimerel, C., L. Movileanu, …, U. Kleinekathöfer. 2008. Transport at the nanoscale: temperature dependence of ion conductance. *Eur. Biophys. J.* 38:121–125.
33. Pezeshki, S., C. Chimerel, …, U. Kleinekathöfer. 2009. Understanding ion conductance on a molecular level: an all-atom modeling of the bacterial porin OmpF. *Biophys. J.* 97:1898–1906.

34. Begic, S., and E. A. Worobec. 2006. Regulation of *Serratia marcescens* OmpF and OmpC porin genes in response to osmotic stress, salicylate, temperature and pH. *Microbiology*. 152:485–491.

35. Mahendran, K. R., C. Chimerel, …, M. Winterhalter. 2009. Antibiotic translocation through membrane channels: temperature-dependent ion current fluctuation for catching the fast events. *Eur. Biophys. J.* 38:1141–1145.

36. Zakharian, E., and R. N. Reusch. 2003. Outer membrane protein A of *Escherichia coli* forms temperature-sensitive channels in planar lipid bilayers. *FEBS Lett.* 555:229–235.

37. Baslé, A., R. Iyer, and A. H. Delcour. 2004. Subconductance states in OmpF gating. *Biochim. Biophys. Acta.* 1664:100–107.

38. Chen, M., S. Khalid, …, H. Bayley. 2008. Outer membrane protein G: engineering a quiet pore for biosensing. *Proc. Natl. Acad. Sci. USA.* 105:6272–6277.

39. Benz, R. 2004. Bacterial and Eukaryotic Porins. Wiley-VCH, Weinheim, Germany.

40. Jung, Y., H. Bayley, and L. Movileanu. 2006. Temperature-responsive protein pores. *J. Am. Chem. Soc.* 128:15332–15340.

41. Kang, X.-F., L.-Q. Gu, …, H. Bayley. 2005. Single protein pores containing molecular adapters at high temperatures. *Angew. Chem. Int. Ed.* 44:1495–1499.

42. Montal, M., and P. Mueller. 1972. Formation of bimolecular membranes from lipid monolayers and a study of their electrical properties. *Proc. Natl. Acad. Sci. USA.* 69:3561–3566.

43. Lindsey, H., N. O. Petersen, and S. I. Chan. 1979. Physicochemical characterization of 1,2-diphytanoyl-*sn*-glycero-3-phosphocholine in model membrane systems. *Biochim. Biophys. Acta.* 555:147–167.

44. Phillips, J. C., R. Braun, …, K. Schulten. 2005. Scalable molecular dynamics with NAMD. *J. Comput. Chem.* 26:1781–1802.

45. MacKerell, A., D. Bashford, …, M. Karplus. 1998. All-atom empirical potential for molecular modeling and dynamics studies of proteins. *J. Phys. Chem. B.* 102:3586–3616.

46. Varma, S., S. W. Chiu, and E. Jakobsson. 2006. The influence of amino acid protonation states on molecular dynamics simulations of the bacterial porin OmpF. *Biophys. J.* 90:112–123.

47. Nestorovich, E. M., T. K. Rostovtseva, and S. M. Bezrukov. 2003. Residue ionization and ion transport through OmpF channels. *Biophys. J.* 85:3718–3729.

48. Müller, D. J., and A. Engel. 1999. Voltage and pH-induced channel closure of porin OmpF visualized by atomic force microscopy. *J. Mol. Biol.* 285:1347–1351.

49. Ceccarelli, M., and P. Ruggerone. 2008. Physical insights into permeation of and resistance to antibiotics in bacteria. *Curr. Drug Targets.* 9:779–788.

50. Humphrey, W. F., A. Dalke, and K. Schulten. 1996. VMD: visual molecular dynamics. *J. Mol. Graph.* 14:33–38, 27–28.